

SUPPORTING INFORMATION

Dehydrogenation Mechanisms of Methyl-cyclohexane on γ -Al₂O₃ Supported Pt₁₃: Impact of Cluster Ductility

Wei Zhao,^{1,2} Céline Chizallet,¹ Philippe Sautet,^{2,3} Pascal Raybaud^{1,}*

¹ IFP Energies nouvelles,

Rond-point de l'échangeur de Solaize, BP 3 - 69360 Solaize, France

² Université de Lyon, CNRS, Laboratoire de Chimie, Ecole Normale Supérieure de Lyon, 46

allée d'Italie, 69364 Lyon cedex 07, France

³ Chemical and Biomolecular Engineering department, Chemistry and Biochemistry

department and CNSI, University of California Los Angeles

Emails: christophezhao628@gmail.com, celine.chizallet@ifpen.fr,

sautet@ucla.edu, pascal.raybaud@ifpen.fr

* Corresponding author: Pascal Raybaud, pascal.raybaud@ifpen.fr, phone:
+33.4.37.70.23.20, fax: +33.4.37.70.20.66

1. Stability of 4-MCHe as a function of the adsorption site (PBE level)

Table S1. Calculated energy, and distances for different 4-MCHe adsorption modes at different adsorption sites (PBE level)

Adsorption Site(s)	Most stable adsorption mode	Number of adsorption conformations calculated	Energy* (kJ/mol)	$d_{C3-C4}(\text{\AA})$	$d_{C3-M}(\text{\AA})$	$d_{C4-M}(\text{\AA})$
V1	π	6	19	1.41	2.23	2.22
V2	π	6	52	1.42	2.17	2.22
V3	π	6	0*	1.42	2.17	2.17
V4	π	1	39	1.43	2.18	2.14
V5	π	5	23	1.41	2.24	2.24
V6**	π	2	67	1.43	2.17	2.17
S2	π	3	31	1.43	2.12	2.13
S6	π	2	56	1.43	2.13	2.11
S7	π	2	98	1.40	2.27	2.33
V1-V2	di- σ	2	65	1.50	2.10	2.10
V2-V3	di- σ	2	40	1.48	2.14	2.13
V2-V5	di- σ	2	78	1.44	2.26	2.27
V3-V5	di- σ	2	42	1.46	2.12	2.17
V5-V6***	di- σ	2	41	1.50	2.13	2.10
V1-V4	di- σ	2	30	1.48	2.20	2.13
V4-V6	di- σ	2	95	1.50	2.12	2.12
V4-V5	di- σ	3	104	1.46	2.21	2.25
V2-V4	di- σ	2	97	1.50	2.17	2.15
V3-S2	di- σ	3	40	1.49	2.10	2.10
V2-S2	di- σ	2	37	1.48	2.10	2.10

*: Total energy of the most stable configurations with V3 site chosen as reference

: The conformation involves the displacement of atom H6 from a top position on V6 to a bridge position between V4 and S6 (see **Figure 1 for the notation in the main text)

***: The conformation involves the displacement of atom H6 from a top position on V6 to a bridge position between V6 and S6 (see **Figure 1** for the notation in the main text)

It is shown that the most stable adsorption mode for 4-methyl-cyclohexene is always the π mode on site V3, which exhibits a minimum energy chosen as reference in **Table S1**.

This result is probably due to the fact that the V3 site has less hydrogen atoms surrounded and causes a lower steric hindrance for the adsorption of the molecule. It is also observed that the π mode is generally more favored than di- σ mode for a given site. For example, the di- σ mode on both V3 and V5 sites exhibits an energy which is far more endothermic than the two adsorptions in π modes on the V3 and V5 sites (43 kJ/mol vs 0 and 23 kJ/mol) .

The C3-C4 average distance for the π mode (1.42 Å) is much shorter than for the di- σ mode (1.48 Å). The C3-C4 (double bond) distance for the isolated methyl-cyclohexene molecule in gaseous phase measures 1.34 Å. This implies that the energy cost induced by the deformation of the molecule is likely higher in the di- σ mode. Meanwhile, the carbon-metal average distances for the di- σ mode (2.15 Å) is shorter than for the π mode (2.19 Å), which suggests that the di- σ bonded molecule exhibits higher interaction strength than π -bonded molecule. However, the compromise between carbon-carbon bonds and carbon-metal bonds makes the π mode generally more favored than di- σ mode on the cluster.

2. Stability of 4-MCHe as a function of conformation (PBE level)

Table S2. Calculated energies and bond lengths for the adsorbed 4-MCHe with the π mode on the V3 site for various conformations (PBE level).

The corresponding molecular structures are given in Figure S1.

Adsorption Site	Adsorption mode	Energy* (kJ/mol)	$d_{C3-C4}(\text{\AA})$	$d_{C3-M}(\text{\AA})$	$d_{C4-M}(\text{\AA})$
V3-1	π	11	1.42	2.18	2.20
V3-2	π	4	1.41	2.19	2.19
V3-3	π	16	1.43	2.18	2.14
V3-4	π	12	1.41	2.25	2.17
V3-5	π	16	1.41	2.30	2.16
V3-6	π	0	1.42	2.17	2.17

*Total energy with reference chosen for the V3-6 configuration.

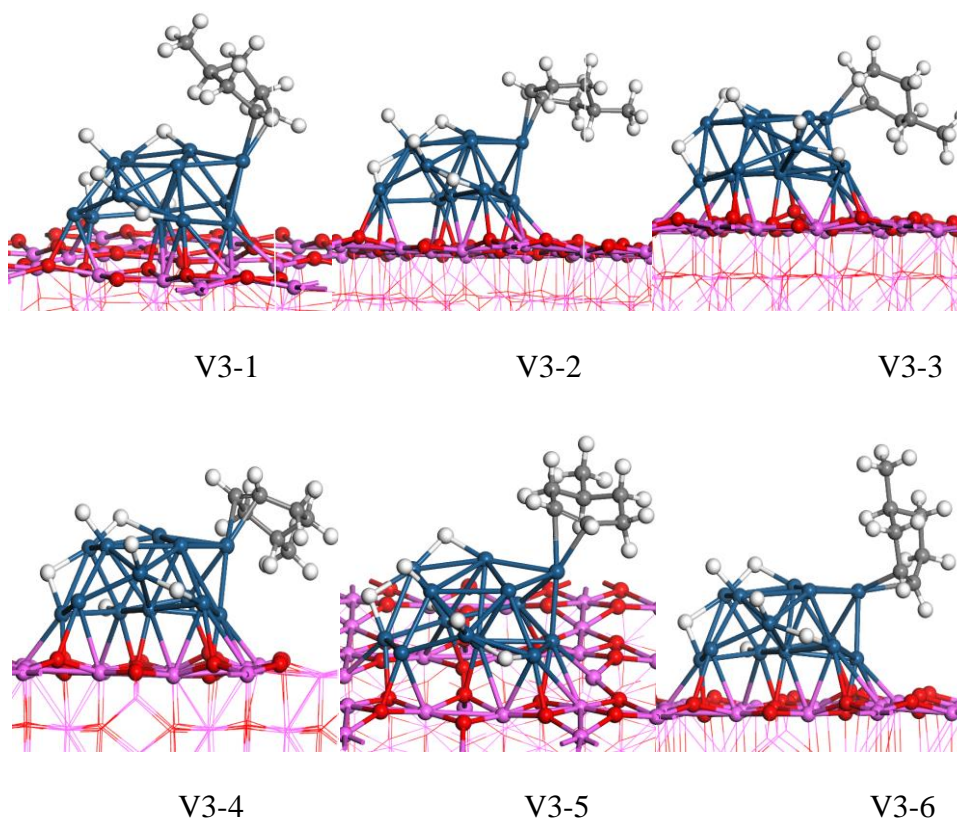


Figure S1. Different conformations for the adsorbed 4-MCHe with the π mode on the V3 site (PBE level). The corresponding energy data are given at the PBE level in Table S2.
Color legend: aluminum (pink balls), oxygen (red balls), platinum (dark blue balls), carbon (dark grey balls), hydrogen (white balls)

It should be emphasized that these conformations were obtained by merely rotating the molecule from their initial positions. It is noticed that the energy variation remains within an interval of 16 kJ/mol. While the molecule rotates around the axis perpendicular to the π -bond, the energy is minimized when the carbon-metal distances are also minimized and well symmetric (2.17 and 2.19 Å, for V3-6 and V3-2 respectively). For the less stable conformation V3-5, the difference between these two distances reaches 0.14 Å. In addition, for the most stable cases (V3-6 and V3-2), the methyl group of the molecule remains the furthest from the cluster and from the support surface, which may thus minimize the steric hindrance.

3. Molecular dynamics simulation of the adsorbed 4-MCHe intermediate

Ab initio molecular dynamics approach was performed at 3 distinct temperatures (500K, 800K and 1200K) for 4-MCHe adsorbed $\text{Pt}_{13}\text{H}_6/\gamma\text{-Al}_2\text{O}_3(100)$ on the V3 site, starting from the most stable configuration (**Figure S1, V3-6**).

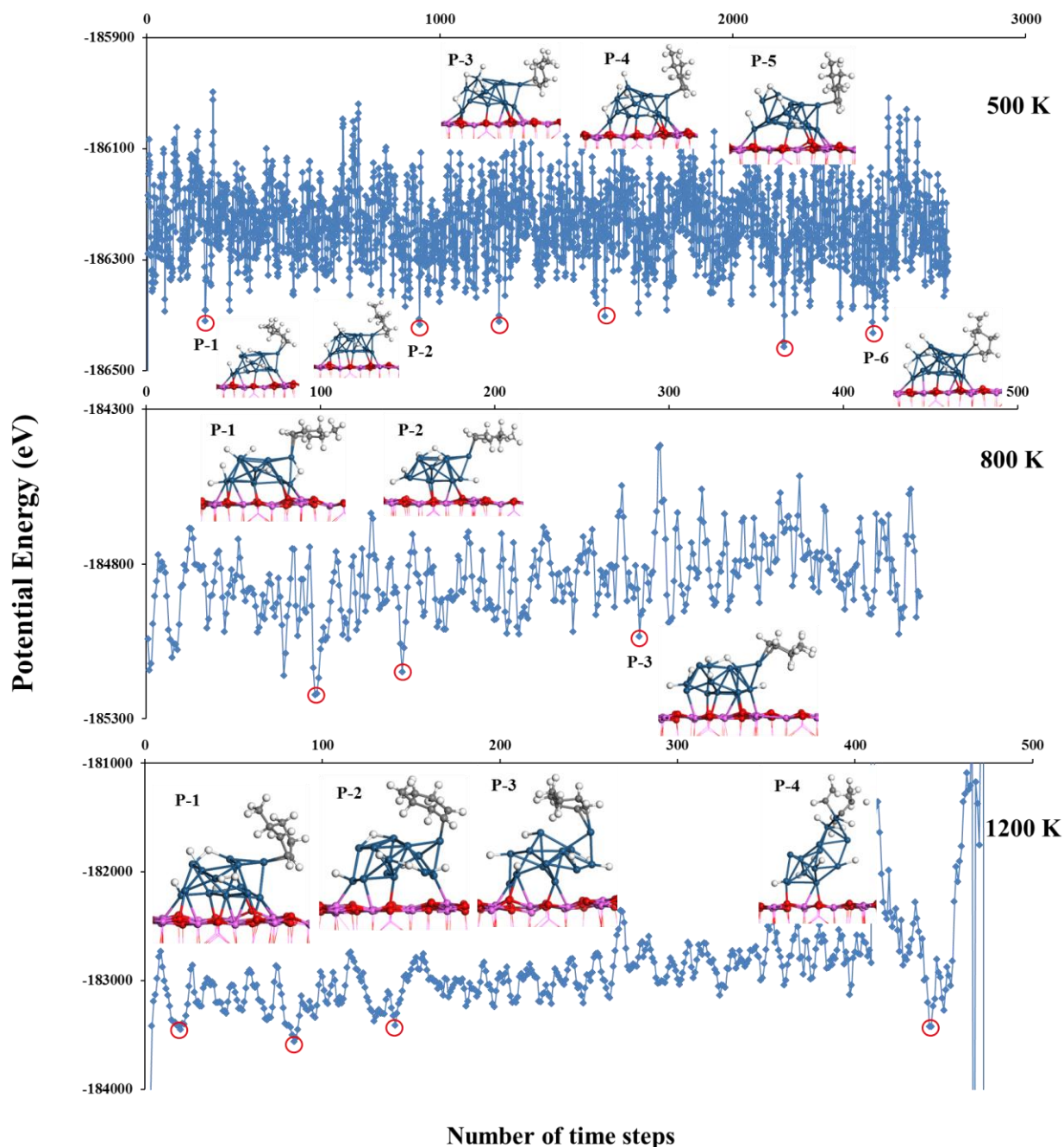


Figure S2. Potential energy (PBE level) as a function of time steps during AIMD for 4-MCHe- $\text{Pt}_{13}\text{H}_6/\gamma\text{-Al}_2\text{O}_3(100)$ where 4-MCHe is adsorbed on the V3 site: (a) 500 K; (b) 800K; (c) 1200K. The structures correspond to the local energy minima shown by red circles and labeled “P-n”. Color legend: aluminum (pink balls), oxygen (red balls), platinum (dark blue balls), carbon (dark grey balls), hydrogen (white balls)

Depending on temperature, the potential energy fluctuates in a more or less large interval. The energy range is about 400 kJ/mol, 800 kJ/mol and over 1200 kJ/mol at $T = 500$, 800 K, and 1200 K respectively. Moreover, at 1200K the system is rapidly destroyed (at $t > 500$ fs). This explains why we extract less points to be quenched on the profile at $T=1200$ K than at $T=500$ K.

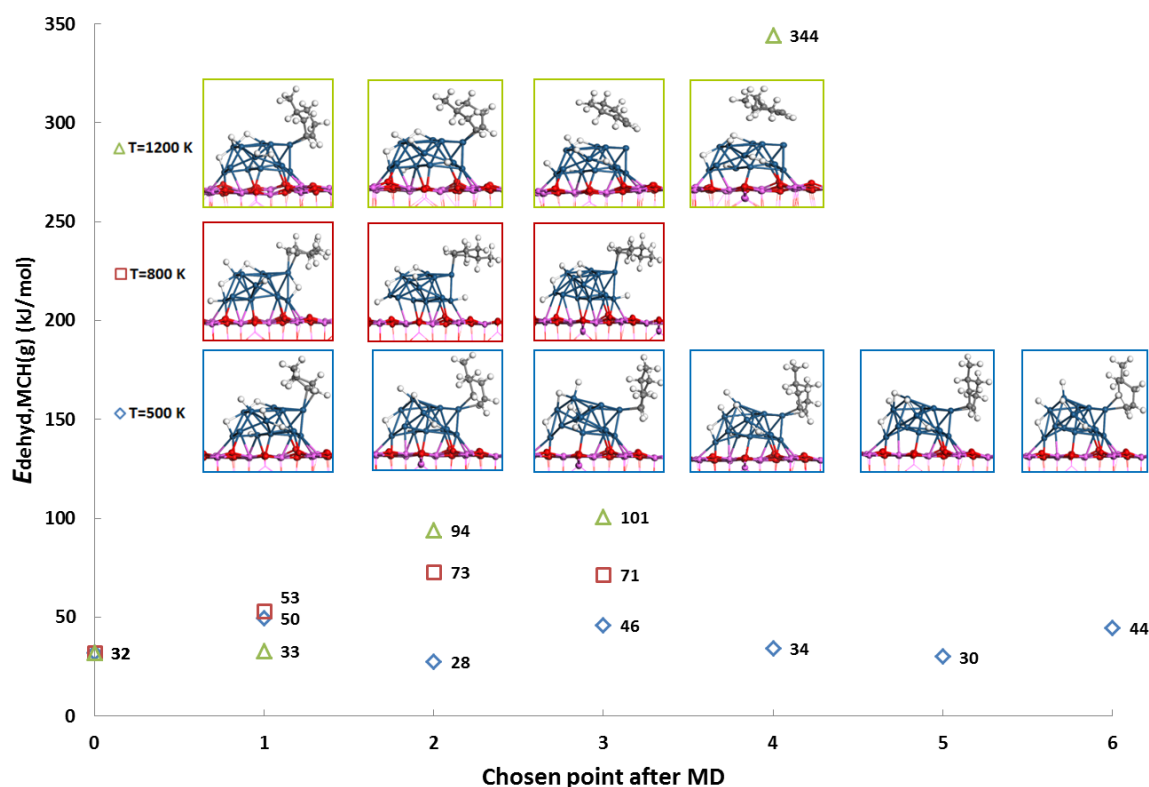


Figure S3. Calculated dehydrogenation electronic energy (PBE level) after quenching the points chosen in Figure S3 after AIMD at 500, 800 and 1200 K. P-0: initial system before MD calculation. The structures correspond to the optimized geometry after quench. Color legend: aluminum (pink balls), oxygen (red balls), platinum (dark blue balls), carbon (dark grey balls), hydrogen (white balls).

Figure S3 presents the dehydrogenation electronic energies for the quenched configurations chosen along the AIMD trajectory, after quench. Quenching the systems from the MD at 500 K leads to lower energy values compared to 800 and 1200 K. In particular, two new configurations are found at 500 K which exhibit lower energies than the starting configuration (obtained from the static approach). The P-2 configuration leads to a dehydrogenation energy

of methyl-cyclohexane(g) to 4-methyl-cyclohexene equal to 28 kJ/mol and will be considered as the most stable system for the further study. The temperatures 800 K and 1200 K are probably too high and induce a progressive destabilization of the molecule (even after quench), which slightly desorbed from the cluster as illustrated by the insets in **Figure S3**. Consequently, for all other intermediates studied in the manuscript, AIMD calculations are systematically undertaken at T=500 K.

4. Evaluation of enthalpic and entropic terms according to statistical thermodynamics

In order to evaluate free energies, we applied *first principles* thermodynamic calculations derived from the vibrational frequency calculations, the latter being performed with VASP. The Gibbs free energy, G , is expressed as a function of the enthalpy H and entropy S of the system:

$$G = H - TS \quad (3)$$

The molar enthalpy of the system is expressed as follows:

$$H = U_{elec} + U_{vib} + U_{trans} + U_{rot} + PV_m \quad (4)$$

Where U_{elec} , U_{vib} , U_{trans} , U_{rot} and V_m are respectively the electronic energy, vibrational energy, translational energy, rotational energy and the molar volume. The molar volume term PV_m was considered for an ideal gas system and for condensed phase systems, H was assimilated to U . The electronic energy was obtained by DFT calculations, other energy terms were calculated from statistical thermodynamics.

Vibrational energy is obtained by knowing all of the vibrational frequencies of the system using the formula:

$$U_{vib}(T) = N_A \left[\sum_i \frac{1}{2} h \nu_i + \sum_i \frac{h \nu_i \times e^{-\frac{h \nu_i}{k_B T}}}{1 - e^{-\frac{h \nu_i}{k_B T}}} \right] \quad (S1)$$

Where h is Planck's constant, k_B is the Boltzmann constant and T the absolute temperature. The first term of $U_{vib,m}$ corresponding to the vibrational energy of the system at 0K and is called "Zero Point Energy".

Rotational and translational components of the internal energy have an analytical expression in the case of ideal gas:

$$U_{trans}(T) = U_{rot}(T) = \frac{3}{2} N_A k_B T \quad (S2)$$

$$\text{For a linear molecule: } U_{rot}(T) = N_A k_B T \quad (S3)$$

Similarly, the molar entropy energy of system can be written as follows:

$$S = S_{vib} + S_{trans} + S_{rot} \quad (5)$$

Where S_{vib} , S_{trans} and S_{rot} are respectively the molar vibrational, translational and rotational entropy which were also calculated from statistical thermodynamics.

From the vibrational frequencies, we calculate the vibrational entropy:

$$S_{vib}(T) = N_A k_B \left[\sum_i \frac{\frac{h\nu_i}{k_B T} \times e^{-\frac{h\nu_i}{k_B T}}}{1 - e^{-\frac{h\nu_i}{k_B T}}} - \sum_i \ln(1 - e^{-\frac{h\nu_i}{k_B T}}) \right] \quad (S4)$$

For rotational and translational components in the case of an ideal gas, the following formula are used:

$$S_{trans}(T) = \frac{5}{2} N_A k_B + N_A k_B \ln \left[\frac{(2\pi M k_B T)^{\frac{3}{2}} V}{N_A h^3} \right] \quad (S5)$$

Where P is the partial pressure of the gas, M is molar mass (formula Sackur-Tetrode)^{100–102} and

$$S_{rot}(T) = N_A k_B \left(\frac{3}{2} + \ln \left[\frac{\sqrt{\pi}}{\sigma} \left(\frac{8\pi^2 k_B T}{h^2} \right)^{\frac{3}{2}} \sqrt{A_e \times B_e \times C_e} \right] \right) \quad (S6)$$

Where A_e , B_e and C_e are the rotational constants of the molecule, and σ is the symmetry number.

For the molecules adsorbed on the cluster, it was assumed that the translation and rotation modes are converted into vibration modes, and thus the associated enthalpy and entropy were included in the vibrational energy and entropy.

5. Vibrational frequencies calculations

The vibrational contribution of enthalpies and entropies were determined by vibrational frequencies calculations within the harmonic approximation, using the numerical derivative of the force matrix with a displacement of ± 0.02 Å around the equilibrium atomic positions. All vibrational analyses has been done primarily at the PBE level. For the great majority of intermediates and TS after geometry optimization at the PBE-dDsC level, the structure did not change, we noticed that PBE-dDsC have barely no influence on vibrational frequencies of the corresponding structures. So, we considered the electronic energies calculated with PBE-dDsC and add the vibrational contributions in the enthalpy, entropy and zero-point energy terms calculated with PBE.

However, as described in the main text, we noticed significant geometry changes between PBE and PBE-dDsC for five intermediates formed at the beginning of the reaction pathway: physisorbed methyl-cyclohexane, first C-H cleavage transition state, (methyl-cyclohexyl+H) intermediate, second C-H cleavage transition state and (methyl-cyclohexene+2H) intermediate. In these cases, the vibrational frequencies were calculated at PBE-dDsC level.

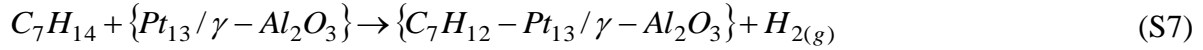
These harmonic vibrational frequency calculations were also performed to evaluate the reliability of the identified transition states (according to the previously described method), whereas one and only one imaginary frequency appears in the frequency calculation corresponding to the reaction coordinate, since it should be a first order saddle point. In order to check the effect of various key parameters of the DFT calculations (cut-off energy, precision, electronic convergence, and forces convergences) we undertook a systematic benchmark reported below. According to this analysis, the calculation with a cut off energy of 400 eV and a “normal” precision leads to Gibbs free energy values in the center of this fluctuation interval with a reasonable computational time and without any spurious imaginary

frequency on the benchmarked system. Thus, we chose these setups as the best compromise and used an electronic convergence criterion of 10^{-6} eV and forces convergence criterion of 0.01 eV/\AA . However, for three systems (adsorbed methyl-cyclohexene, methyl-cyclohexenyl+H and methyl-cyclohexadienyl+H), spurious low vibrational imaginary frequencies remain present. Thus, as proposed by Sabbe et al.,¹ we replaced the frequencies lower than the cutoff value of 50 cm^{-1} and all spurious imaginary frequencies (if any), by the common value of 50 cm^{-1} for the thermodynamic calculations of all supported systems. We also evaluated the impact of this approximation on the TS_{vib} values for systems which do not exhibit any spurious imaginary frequencies. The intrinsic TS_{vib} values are systematically downshifted by about 12-30 kJ/mol at 625 K, if we replace the frequencies smaller than 50 cm^{-1} by the cutoff frequency. Simultaneously, $T\Delta S_{vib}$ values for the adsorption of MCH and desorption steps of toluene and H_2 are impacted by less than 17 kJ/mol, respectively, depending on the use of the cutoff frequency or not. For the other elementary steps involving much less change in the vibrational soft modes are impacted by less than 10 kJ/mol at 625 K.

Optimization of the DFT parameters for vibrational calculations

We attempted different parameters combination “packages” in terms of cut-off energy (400, 500, 600 eV), precision flag in VASP (normal, accurate, high), electronic convergence criterion (10^{-5} , 10^{-6} , 10^{-8} eV) and forces convergence criterion (0.01, 0.02 eV/ \AA) to optimize the adsorbed methyl-cyclohexene system for bench-marketing (reaction presented in **Equation(S7)**), since that this is one of the crucial reaction intermediate considered in our mechanism later. These tests were done to probe if there is a potential connection between the extinction of these parasite imaginary frequencies and the calculation parameters. Among all the parameters choices applied on the methyl-cyclohexene adsorbed system, it turns out only five parameter “packages” managed to eliminate these imaginary frequencies: (1) cut-off

energy = 400 eV; normal precision; electronic convergence criterion = 10^{-5} eV; forces convergence criterion = 0.02 eV/Å; (2) cut-off energy = 400 eV; normal precision; electronic convergence criterion = 10^{-5} eV; forces convergence criterion = 0.01 eV/Å; (3) cut-off energy = 500 eV; normal precision; electronic convergence criterion = 10^{-5} eV; forces convergence criterion = 0.01 eV/Å; (4) cut-off energy = 400 eV; normal precision; electronic convergence criterion = 10^{-8} eV; forces convergence criterion = 0.005 eV/Å; (5) cut-off energy = 400 eV; accurate precision; electronic convergence criterion = 10^{-8} eV; forces convergence criterion = 0.005 eV/Å. Sometimes, with more severe optimization parameters (ex. high cut-off energy and precision, 600 eV), the extinction of parasite imaginary frequencies is not guaranteed. However, the cut-off energy = 400 eV at normal precision are constantly efficient. In addition, stringent electronic and forces convergence criteria are also recommended by our tests for the extinction of these parasite imaginary frequencies (tests (4) and (5)). Nevertheless, these stringent criteria demand relatively long calculation time.



On the other hand, the contribution of these small parasite imaginary frequencies, which are converted from negative eigenvalue to positive by DFT at the end of calculation, can be tremendous and uncertain to the vibrational entropy term if no proper countermeasures are adopted. This can be seen by the expression of vibrational entropy term in **Equation (S8)**,

$$\text{When } v_i \rightarrow 0, \text{ we have } \frac{\frac{h\nu_i}{k_B T} \times e^{-\frac{h\nu_i}{k_B T}}}{1 - e^{-\frac{h\nu_i}{k_B T}}} \rightarrow 1 \text{ and } \ln(1 - e^{-\frac{h\nu_i}{k_B T}}) \rightarrow -\infty, \text{ so } S_{vib,i} \rightarrow +\infty.$$

$$S_{vib,i} = N_A k_B \left[\frac{\frac{h\nu_i}{k_B T} \times e^{-\frac{h\nu_i}{k_B T}}}{1 - e^{-\frac{h\nu_i}{k_B T}}} - \ln(1 - e^{-\frac{h\nu_i}{k_B T}}) \right] \quad (S8)$$

An analysis of the vibrational frequencies was thus done to evaluate the entropy deviation induced by the soft modes and imaginary frequencies obtained by different calculation parameters for methyl-cyclohexene system at reforming temperature $T = 800$ K. The last five vibrational frequencies coming out from the DFT calculations are listed in **Table S3**, which includes soft modes and imaginary frequencies (underlined value) that are converted from negative eigenvalue to positive by DFT at the end of calculation. Here in **Table S3**, three parameter “packages” (with same electronic convergence criterion = 10^{-5} eV and forces convergence criterion = 0.02 eV/Å, for the sake of calculation time) were chosen to make a comparison: (a) cut-off energy = 400 eV; normal precision; (b) cut-off energy = 400 eV; High precision; (c) cut-off energy = 500 eV; normal precision. These three cases were representative among all because the case (a) has no parasite imaginary frequencies, while the cases (b) and (c) reveals the most significant (\pm) deviation on total vibrational entropy at 800 K compared to (a) during our analysis, due to the apparition of parasites imaginary frequencies. The vibrational entropy corresponding to each frequency is calculated by using **Equation (S8)**. It indicates thereby from **Table S3** that the apparition of these soft modes or imaginary frequencies contributes by $-20 \sim +3$ kJ/mol to the vibrational entropies term TS_{vib} at 800 K.

Table S3. Frequency analysis for the contributions of the last five soft modes and imaginary frequencies to the vibrational entropies at T=800 K calculated at PBE level
(The underlined values correspond to imaginary frequencies)

	E_{cut-off} =400 eV		E_{cut-off} =400 eV		E_{cut-off} =500 eV	
	normal precision		high precision		normal precision	
	ν_i (cm ⁻¹)	$TS_{vib,i}$ (kJ/mol)	ν_i (cm ⁻¹)	$TS_{vib,i}$ (kJ/mol)	ν_i (cm ⁻¹)	$TS_{vib,i}$ (kJ/mol)
Last five vibrational frequencies	38.98	30.4	29.91	32.6	35.78	31.1
	35.97	31.1	29.21	32.8	26.16	33.7
	29.21	32.8	17.88	36.9	12.75	39.7
	28.31	33.1	<u>14.69</u>	<u>38.5</u>	<u>83.24</u>	<u>24.1</u>
	11.43	40.6	<u>39.56</u>	<u>30.3</u>	<u>86.22</u>	<u>23.8</u>
$\Sigma \nu_i$ and $\Sigma TS_{vib,i}$	143.9	168	131.3	171	244.2	152
Deviation $\Delta \Sigma$ compared to 1 st column	0	0	-12.7	+3	+100.3	-16

In addition, a recommended method for treating residual imaginary frequencies has been proposed by Sabbe et al.,¹ which is to replace the frequencies lower than a given frequency cutoff by a common value. In line with this previous work, we replaced all frequencies lower than 50 cm⁻¹ and all spurious imaginary frequencies (if any) by 50 cm⁻¹ before thermodynamic calculations. For transition states, the imaginary frequency corresponding to the reaction coordinate and to a first order saddle point has to be eliminated before the Gibbs free energy calculation. The reaction enthalpy and Gibbs free energy for the dehydrogenation

of methyl-cyclohexane (taken in gas phase) to adsorbed methyl-cyclohexene and one molecule H_2 released in gas phase, are reported in **Figure S4**.

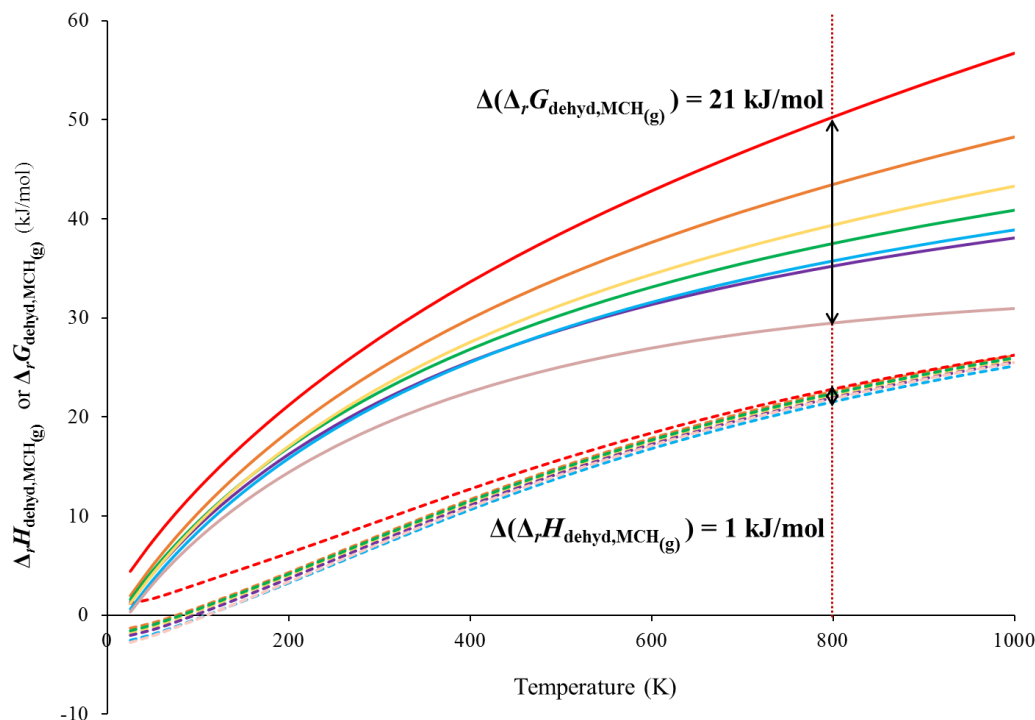


Figure S4. Deviation of dehydrogenation Gibbs energy $\Delta_r G_{\text{dehyd,MCH(g)}}$ (plain lines) and Enthalpy $\Delta_r H_{\text{dehyd,MCH(g)}}$ (dot lines) for the dehydrogenation of methyl-cyclohexane to adsorbed methyl-cyclohexene, using different set of DFT calculations parameters. Curve color legend: $E_{\text{cutoff}} = 500$ eV, normal precision (red); $E_{\text{cutoff}} = 400$ eV, normal precision (orange); $E_{\text{cutoff}} = 500$ eV, accurate precision (yellow); $E_{\text{cutoff}} = 400$ eV, accurate precision (green); $E_{\text{cutoff}} = 500$ eV, high precision (bleu); $E_{\text{cutoff}} = 600$ eV, normal precision (purple); $E_{\text{cutoff}} = 400$ eV, high precision (pink).

We investigated the effect of the energy cutoff (400, 500, 600 eV) and the precision (normal, accurate, high) of the calculation, at same electronic convergence criterion = 10^{-5} eV and forces convergence criterion = 0.02 eV/\AA . It can be noticed in **Figure S4** that the parameters (energy cutoff and precision) used for the calculation strongly impact the Gibbs free energy values, even though after replacing all frequencies lower than 50 cm^{-1} and all spurious imaginary frequencies (if any) by 50 cm^{-1} . It can be seen that the deviation on the

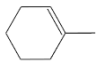
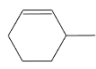
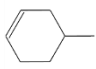
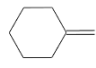

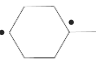

reaction enthalpy is very small, taking the reforming temperature 800 K for a comparison, the deviation is close to 1 kJ/mol, which can be neglected on the final result. However, the deviation on the Gibbs free energy is higher (21 kJ/mol at 800 K). This makes this kind of calculation very sensitive to the chosen parameters in the reforming conditions. This important deviation on the Gibbs free energy is thus due to the vibrational entropic terms, since enthalpies varied very little in our case.

In conclusion, the calculation with rather “standard” parameters of the VASP software (cut off energy of 400 eV, normal precision) leads to Gibbs energy values in the center of this fluctuation interval with a reasonable computational time and without any spurious imaginary frequency, we chose it as the best compromise for further calculations in combination with a slightly more stringent electronic convergence criterion of 10^{-6} eV and forces convergence criterion of 0.01 eV/Å.

6. Molecular structures and energetic stability of C₇H₁₂ intermediates on the γ -Al₂O₃ supported Pt₁₃ cluster (PBE level)

Here, we determine the relative stabilities of C₇H₁₂ intermediates by systematically calculating the dehydrogenation electronic energy (PBE) of the gas phase methylcyclohexane (C₇H₁₄, MCH) into adsorbed C₇H₁₂ plus one gas phase H₂ molecule, keeping the hydrogen coverage constant on the cluster. The corresponding dehydrogenation electronic energies (**Equations (1) and (2)**) have been evaluated for the two sites V3 and V5, chosen according to the dedicated study on the stability of adsorbed 4-MCHe (**supporting information 4**).

Table S4. Dehydrogenation energy of MCH(g) into C₇H₁₂ intermediates on Pt₁₃/ γ -Al₂O₃ (PBE level). The corresponding adsorption modes are illustrated in Figure S5.

	C ₇ H ₁₂	Adsorption mode	Adsorption site(s)	$\Delta_r E_{dehyd, MCH(g)}$ (kJ/mol)
(a)		π	V3	32
(b)		π	V3	44
(c)		π	V3	32
(d)		π	V3	36
(e)		di- σ	V3V5	78
(f)		di- σ	V3V5	77
(g)		di- σ	V3V5	80

Note: The two black dots mean two σ bonds connected with the Pt(V3) and Pt(V5) sites.

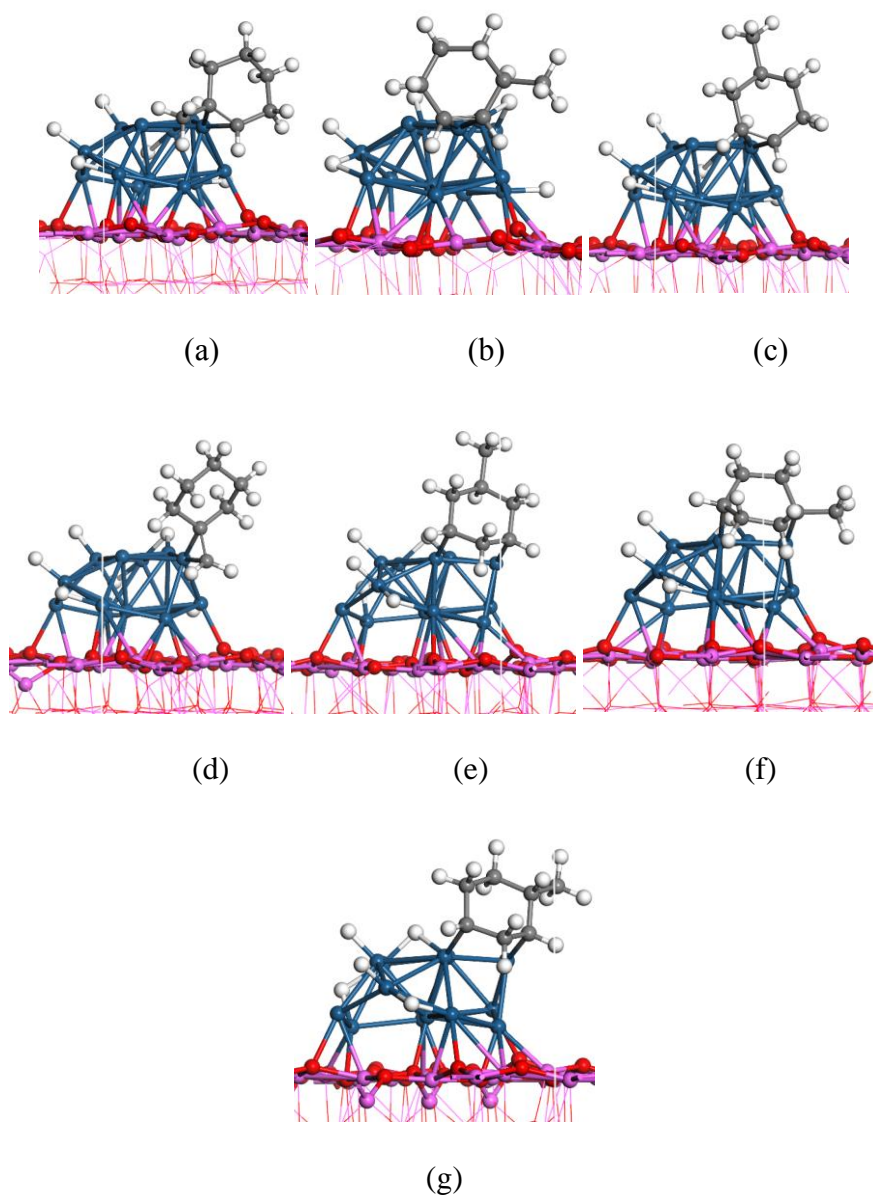


Figure S5. Various dissociative adsorption modes during dehydrogenation of MCH to C_7H_{12} intermediates on the Pt cluster : (a) 1-Methyl-cyclohexene, (b) 3-Methyl-cyclohexene, (c) 4-Methyl-cyclohexene, (d) Methylene-cyclohexane (e) C_3,C_5 -radical, (f) C_1,C_4 -radical, (g) C_2,C_4 -radical. Corresponding energies are given at PBE level in Table S4. Color legend: aluminum (pink balls), oxygen (red balls), platinum (dark blue balls), carbon (dark grey balls), hydrogen (white balls)

7. Molecular structures and energies of key intermediates involved in the dehydrogenation of MCH into toluene (PBE level)

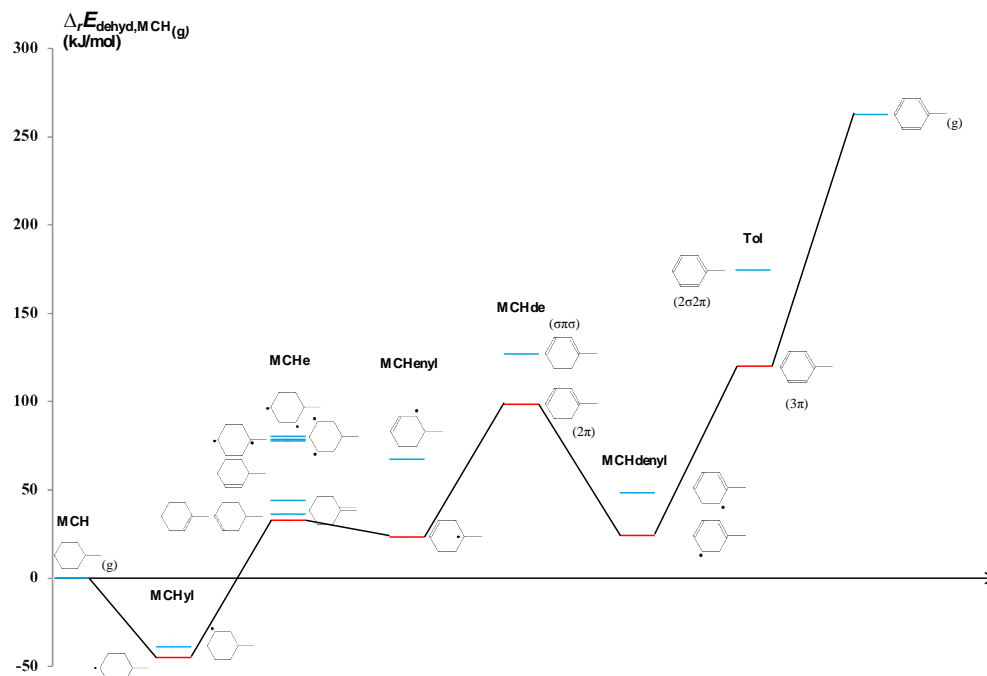


Figure S6. Energy profile at PBE level for various intermediates involved in the dehydrogenation of MCH into toluene (see Figure 2 of the main text)

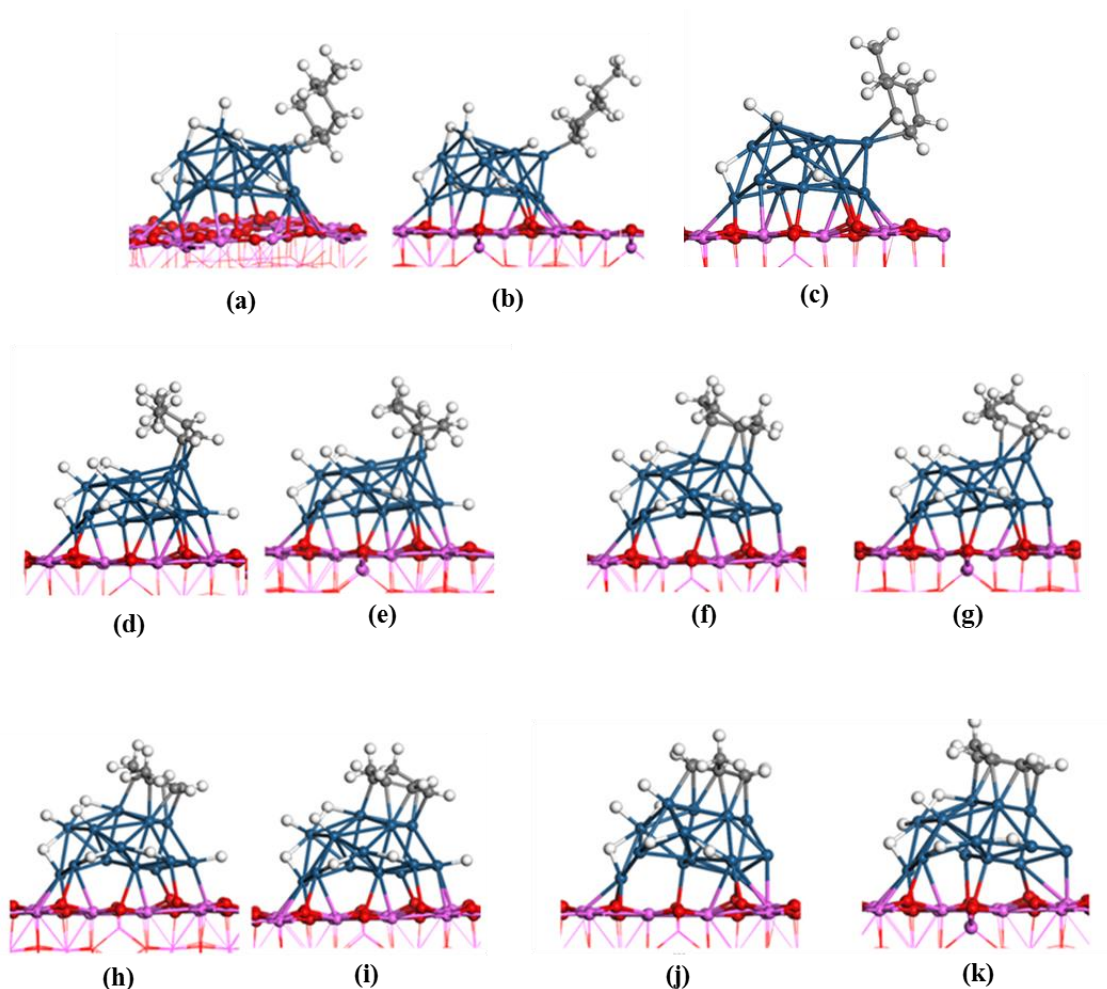


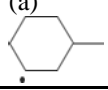
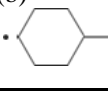
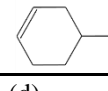
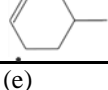
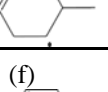
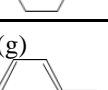
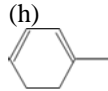
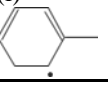
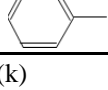
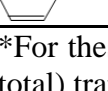

Figure S7. Stable adsorption modes (PBE level) of each intermediate on $\text{Pt}_{13}\text{H}_6/\gamma\text{-Al}_2\text{O}_3$ (100) :

- (a) Methyl-cyclohexyl C3- σ , (b) Methyl-cyclohexyl C4- σ ; (c) 4-Methyl-cyclohexene;
 (d) Methyl-cyclohexenyl $\pi\sigma$ (conjugated) (e) Methyl-cyclohexenyl $\pi\sigma$;
 (f) Methyl-cyclohexadiene 1,4-di- σ -2,3- π (g) Methyl-cyclohexadiene 2 π ;
 (h) Methyl-cyclohexadienyl C5- $\sigma\pi\pi$
 (i) Methyl-cyclohexadienyl C6- $\sigma\pi\pi$; (j) Toluene bri-2 π 2 σ (k) Toluene 3 π .

Color legend: aluminum (pink balls), oxygen (red balls), platinum (dark blue balls), carbon (dark grey balls), hydrogen (white balls).

It must be noticed that the π mode adsorption is the predominant adsorption mode for 4-MCHe, methyl-cyclohexadiene and toluene. Ma et al.² and Morin et al.^{3,4} found that for 1,3-cyclohexadiene and benzene on Pt (111) surface, the most stable adsorption modes are 1,4-di- σ -2,3- π and bri 2 π 2 σ , respectively. These results highlight the specific behavior of the cluster.

Table S5. Adsorption modes, sites and dehydrogenation energies (kJ/mol) for key intermediates on Pt₁₃H₆/γ-Al₂O₃ (100) along the path depicted in Figure S6.

Intermediates	Adsorption mode	Adsorption site	$\Delta E_{\text{dehyd,MCH(g)}}$ (PBE level)	$\Delta E_{\text{dehyd,MCH(g)}}$ (PBE-dDsC)
(a) 	σ	V3	-40	nc
(b) 				
(c) 	π	V3	28	3
(d) 	$\pi\sigma$ (conjugated)	V3-V5	23	-4
(e) 				
(f) 	$\sigma\pi\sigma$	V2-V3-V5	127	nc
(g) 	2π	V3-V5	98	73
(h) 	$\pi\pi\sigma$	V2-V3-V5	24	-1
(i) 				
(j) 	bri- $2\pi 2\sigma$	V2-V3-V4-V5	174	
(k) 	3π	V2-V3-V5	120	104

*For these intermediates, the cluster contains one more hydrogen atom (7 hydrogen atoms in total) transferred from the molecule.

nc: not calculated

8. Thermodynamic data of the energy profiles of MCH dehydrogenation on $\text{Pt}_{13}\text{H}_6/\gamma\text{-Al}_2\text{O}_3$ (100) at different temperatures

Table S6. MCH dehydrogenation energies, enthalpies, entropies and free energies (in kJ/mol) on $\text{Pt}_{13}\text{H}_6/\gamma\text{-Al}_2\text{O}_3$ (100) at different temperatures calculated at the PBE-dDsC level.

Intermediates and transition states	0 K	625 K			800 K		
	$\Delta_r E^*$	$\Delta_r H^*$	$T\Delta_r S^*$	$\Delta_r G^*$	$\Delta_r H^*$	$T\Delta_r S^*$	$\Delta_r G^*$
(A) Methyl-cyclohexane	-45	-40	-91	51	-37	-113	76
TS_a	-14	-21	-105	83	-18	-131	112
(B) Methyl-cyclohexyl + H	-87	-88	-97	9	-84	-120	36
TS_b	1	-15	-94	79	-11	-116	105
(C) Methyl-cyclohexene + 2H	-105	-116	-94	-21	-111	-115	4
(D) Methyl-cyclohexene	3	-13	-20	7	-9	-21	12
TS_d	116	85	-17	102	89	-17	106
(E) Methyl-cyclohexenyl + H	9	-19	-32	13	-14	-35	21
TS_e	66	33	-20	54	38	-21	59
(F) Methyl-cyclohexenyl + H	14	-13	-24	11	-8	-24	17
TS_f	82	48	-2	50	53	2	50
(G) Methyl-cyclohexenyl + H	-4	-30	-9	-21	-24	-5	-20
TS_g	44	3	-9	12	8	-5	13
(H) Methyl-cyclohexadiene + 2H	-74	-108	-13	-95	-102	-9	-92
(I) Methyl-cyclohexadiene	73	33	68	-35	39	94	-55
TS_i	100	53	68	-15	57	92	-35
(J) Methyl-cyclohexadiene	74	34	58	-25	39	81	-42
TS_j	119	68	48	20	73	67	6
(K) Methyl-cyclohexadienyl + H	33	-18	65	-83	-11	91	-102
TS_k	88	30	71	-41	36	97	-61
(L) Methyl-cyclohexadienyl + H	-1	-48	57	-106	-42	81	-122
TS_l	107	46	65	-19	52	90	-38
(M) Toluene + 2H	-23	-78	73	-151	-71	102	-172
(N) Toluene	104	45	131	-86	51	175	-124
Toluene (gas phase)	283	219	262	-42	222	338	-116

*In this table, $\Delta_r X$ stands for $\Delta_r X_{dehyd, MCH(g)}$ according to the notation defined in the main text.

Table S7. MCH dehydrogenation energies, enthalpies, entropies and free energies (in kJ/mol) on Pt₁₃H₆/γ-Al₂O₃ (100) at different temperatures calculated at the PBE level.

Intermediates and transition states	0 K	625 K			800 K		
	$\Delta_r E$	$\Delta_r H$	$T\Delta_r S$	$\Delta_r G$	$\Delta_r H$	$T\Delta_r S$	$\Delta_r G$
(A) Methyl-cyclohexane	21	25	-83	108	29	-102	131
TS_a	52	44	-95	140	47	-119	166
(B) Methyl-cyclohexyl + H	-43	-44	-94	50	-40	-116	76
TS_b	29	14	-89	103	18	-109	127
(C) Methyl-cyclohexene + 2H	-71	-81	-92	11	-76	-112	36
(D) Methyl-cyclohexene	28	12	-20	32	16	-21	37
TS_d	149	118	-17	135	122	-17	139
(E) Methyl-cyclohexenyl + H	38	10	-32	42	16	-35	51
TS_e	97	65	-20	85	69	-21	90
(F) Methyl-cyclohexenyl + H	44	17	-24	41	22	-24	47
TS_f	111	78	-2	80	82	2	80
(G) Methyl-cyclohexenyl + H	23	-3	-9	6	3	-5	8
TS_g	77	36	-9	45	42	-5	46
(H) Methyl-cyclohexadiene + 2H	-42	-76	-13	-63	-70	-9	-60
(I) Methyl-cyclohexadiene	98	58	68	-10	64	94	-30
TS_i	127	80	68	12	84	92	-7
(J) Methyl-cyclohexadiene	99	59	58	0	64	81	-17
TS_j	145	94	48	46	99	67	32
(K) Methyl-cyclohexadienyl + H	56	6	65	-59	12	91	-78
TS_k	110	53	71	-18	58	97	-39
(L) Methyl-cyclohexadienyl + H	24	-24	57	-81	-17	81	-98
TS_l	129	68	65	3	74	90	-16
(M) Toluene + 2H	2	-53	73	-126	-45	102	-147
(N) Toluene	122	63	131	-68	69	175	-106
Toluene (gas phase)	262	198	262	-63	201	338	-137

*In this table, $\Delta_r X$ stands for $\Delta_r X_{dehyd, MCH(g)}$ according to the notation defined in the main text.

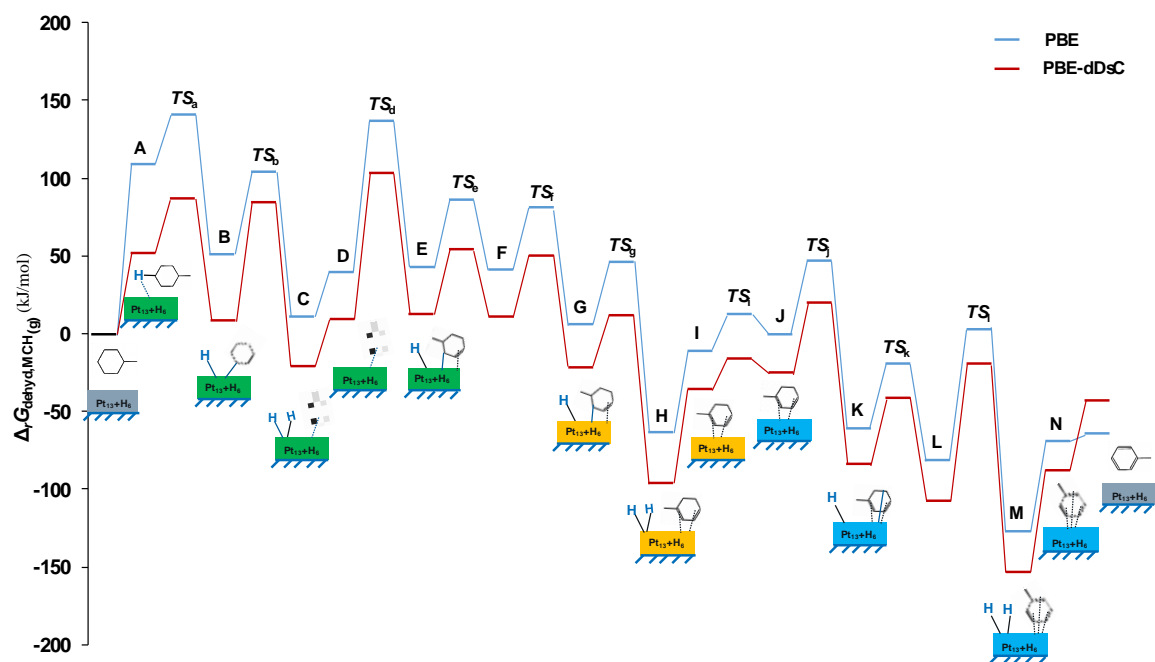


Figure S8. Gibbs free energy profiles for methyl-cyclohexane dehydrogenation reaction mechanism over $\text{Pt}_{13}\text{H}_6/\gamma\text{-Al}_2\text{O}_3$ calculated with the PBE (blue line) and the PBE-dDsC (red line) functionals at 625 K.

9. Complementary data on the elementary steps of the reaction

9.1 Methyl-cyclohexane adsorption, toluene desorption and hydrogen desorption

Table S8. Thermodynamic data (kJ/mol at PBE-dDsC level) for the methyl-cyclohexane adsorption and toluene desorption elementary steps at 625 K

Elementary step	$\Delta_r E$	$\Delta_r H$	$T\Delta_r S$	$\Delta_r G$
MCH (g) \rightarrow A	-45	-40	-91	51
N \rightarrow Tol (g)	179	174	130	44

The formation of intermediate A (step (1)), includes one extra step with a preliminary cluster reconstruction from the original structure to the deformed one. This step is not presented in the reaction energy profiles and is assumed to be merged within one single step (1). The same occurs for the deformed cluster after the last toluene desorption step, from the deformed cluster of N alone to the original cluster alone, the reconstruction occurring at the end of reaction path is also merged with the desorption step (15).

Table S9. Thermodynamic data (in kJ/mol at PBE-dDsC level) of H₂ desorption steps at 625 K

Elementary step	$\Delta_r E$	$\Delta_r H$	$T\Delta_r S$	$\Delta_r G$
C \rightarrow D + H ₂	108	103	74	29
H \rightarrow I + H ₂	147	141	81	60
M \rightarrow N + H ₂	127	124	59	65

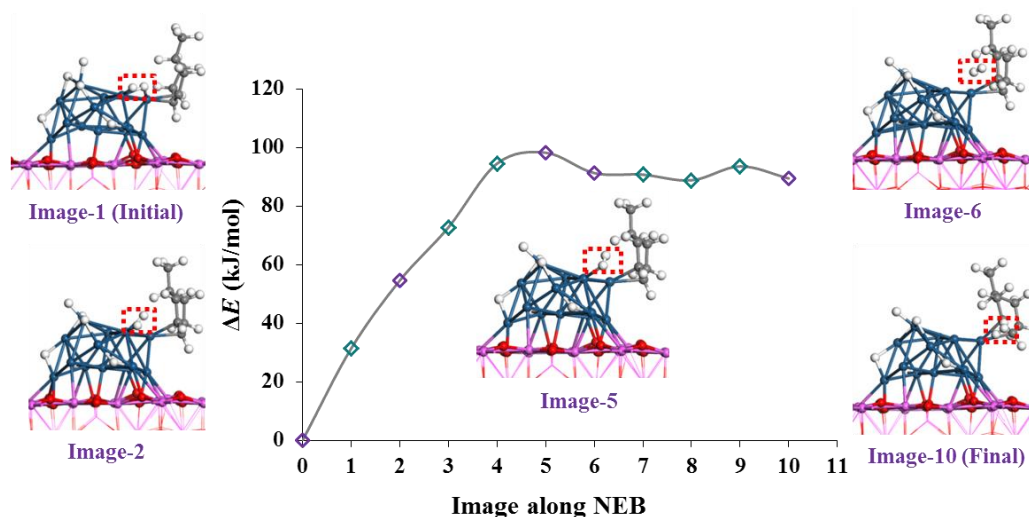


Figure S9. Snapshots and electronic energies images along the NEB performed to simulate the H_2 molecule desorption step $\text{C} \rightarrow \text{D} + \text{H}_2$ (PBE level). Color legend: aluminum (pink balls), oxygen (red balls), platinum (dark blue balls), carbon (dark grey balls), hydrogen (white balls).

To unravel the transition states and activation energies of the H_2 desorption steps, we explored the intermediate states from an initial state with two extra hydrogen atoms on cluster (C) to a final state with a molecule of H_2 formed but remaining close to the cluster, which is a preliminary intermediate just before D. The calculated electronic energies of each image during the NEB are reported in **Figure S9**. This activation step starts with one of the two hydrogen atoms (H_a) moving from a bridge position to a top position, sharing the same platinum atom with the second hydrogen atom (H_b). Then $\text{H}_a - \text{Pt}$ bond breaks and the $\text{H}_a - \text{H}_b$ forms (H_2), while H_b is still on top position of platinum atom. Then the $\text{H}_b - \text{Pt}$ bond breaks as well and the new-formed H_2 is desorbed. After quasi-Newton optimization, the activation energy is found to be +9 kJ/mol (PBE level) greater than the desorption energy only, thus very close to the final state.

Table S10. Thermodynamic and kinetic data for H atom diffusion (PBE-dDsC level) at 625 K

Elementary step	Transition State	Forward reaction								Backward reaction			
		$\Delta_r E$	$\Delta_r H$	$T\Delta_r S$	$\Delta_r G$	$\Delta_r E^\ddagger$	$\Delta_r H^\ddagger$	$T\Delta_r S^\ddagger$	$\Delta_r G^\ddagger$	$\Delta_r E^\ddagger$	$\Delta_r H^\ddagger$	$T\Delta_r S^\ddagger$	$\Delta_r G^\ddagger$
$\text{E} \rightarrow \text{F}$	TS_e	5	6	8	-2	57	53	12	41	52	47	4	43
$\text{K} \rightarrow \text{L}$	TS_k	-34	-30	-8	-23	55	48	6	42	89	78	13	65

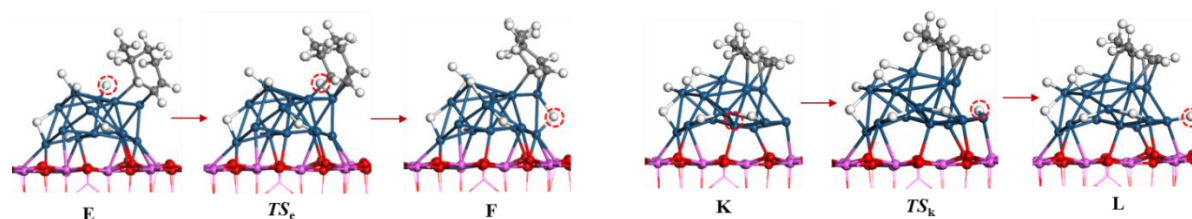


Figure S10. Transition states for H diffusion steps (PBE-dDsC level)

9.2 Cluster reconstructions

Table S11. Thermodynamic and kinetic data for the cluster reconstruction steps (PBE-dDsC level).

Elementary step	Transition States	Forward reaction								Backward reaction			
		$\Delta_r E$	$\Delta_r H$	$T\Delta_r S$	$\Delta_r G$	$\Delta_r E^\ddagger$	$\Delta_r H^\ddagger$	$T\Delta_r S^\ddagger$	$\Delta_r G^\ddagger$	$\Delta_r E^\ddagger$	$\Delta_r H^\ddagger$	$T\Delta_r S^\ddagger$	$\Delta_r G^\ddagger$
Reconstruct. A		35	32	7	25	--				--			
F \rightarrow G	TS_f	-18	-17	15	-32	68	61	22	40	86	78	6	72
I \rightarrow J	TS_i	1	1	-10	11	27	20	0	20	25	19	9	10
Reconstruct. N ₁		-41	-40	-16	-25	--				--			
Reconstruct. N ₂		52	56	-13	70	--				--			

Structural and energetic analysis of the adsorbed 4-MCHe intermediate before and after AIMD

From the AIMD analysis undertaken in **supplementary information S3**, we found two configurations with slightly lower energy (by -2 and -4 kJ/mol, respectively) than the previous one (V3-6) obtained by static approach as described in **supplementary information S3**. The structural data of the lowest energy configuration (by -4 kJ/mol) obtained after AIMD are compared with the structure obtained after static optimization in **Table S12**.

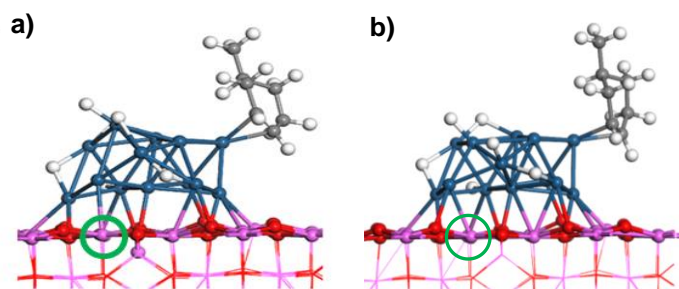


Figure S11. Molecular structure of adsorbed MCHe a) after and b) before AIMD.

Table S12. Most relevant geometrical parameters for the system before and after MD (PBE level)

	After AIMD	Before AIMD
Energy (kJ/mol)	-4	0
H ₆ position	V4	V6
Pt _(V6-S4) distance (Å)	2.79	2.53
* Pt _(S6) -Al distance (Å)	2.62	2.58
Pt _(V3) -C ⁼ distance (Å)	2.15 ; 2.14	2.17 ; 2.17
C=C distance (Å)	1.43	1.42

* : Atom Al stands for the aluminum atom marked by green cycle on the structure images, the one which is linked with the Pt_(S6) before and after MD.

First, it can be noticed that the shape of the metal cluster changed after the MD-quench sequence. The distance between Pt_(V6) and Pt_(S4) atoms is increased by about 0.26 Å. Moreover, the cluster loses part of its bilayer nature, which is the most stable configuration in the absence of any adsorbed molecules.⁵ Meanwhile a migration of one hydrogen (H₆ as

defined in **Figure 1**) atom from site V6 to V4 happened and cluster-support distance are slightly increased (e.g. $\text{Pt}_{(56)}\text{-Al}$ increases by 0.04 Å). Finally, the position of 4-MCHe is also affected: it loses its perpendicular orientation with respect to the alumina surface, and becomes tilted after AIMD with slightly shorter M-C distances.

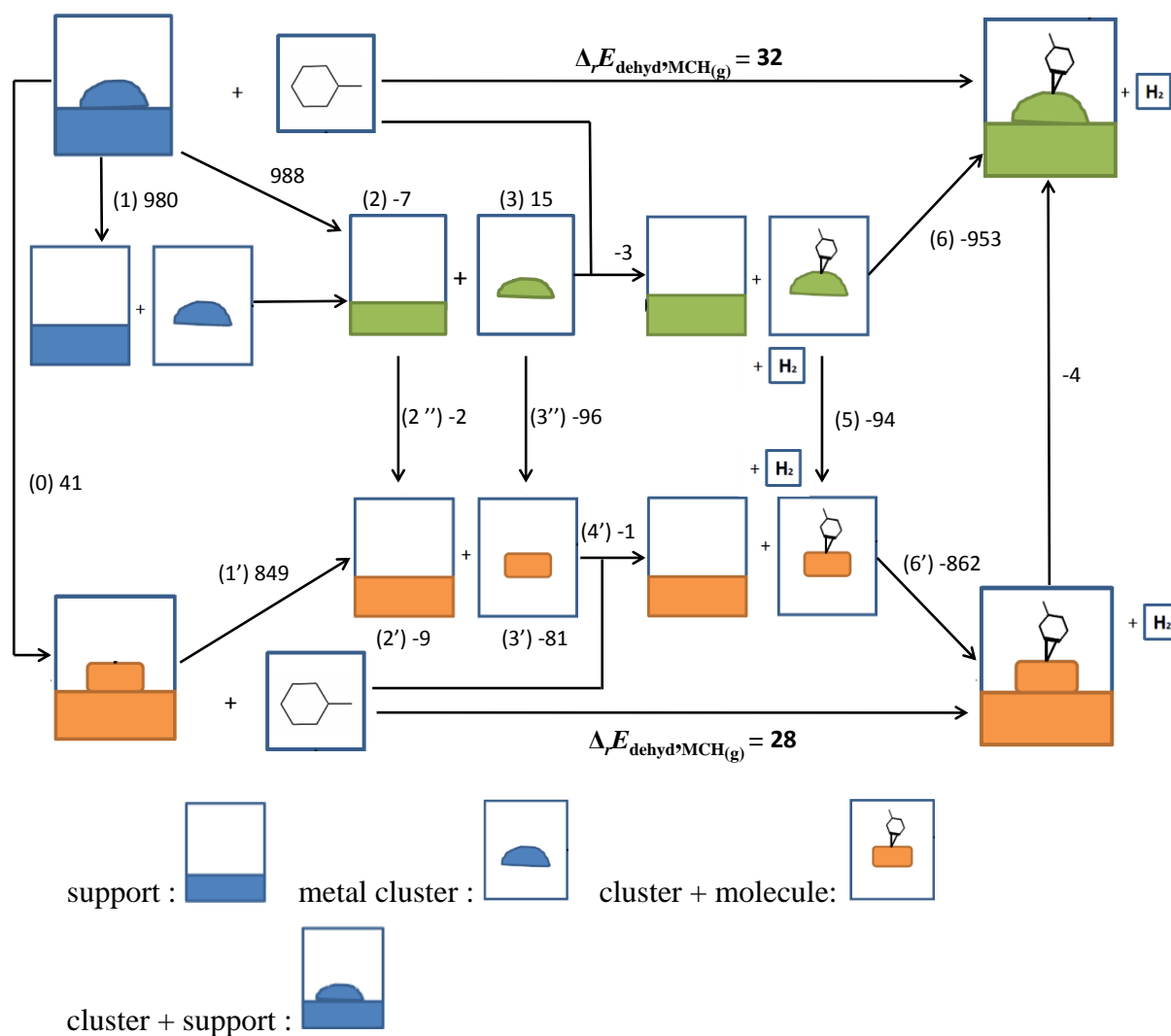


Figure S12. Decomposition of the dehydrogenation energy (in kJ/mol) for adsorbed 4-methylcyclohexene before and after MD. (Color legend: blue : reference system ; green : system before MD; orange : system after MD calculations.)

The energy of each step is marked on each arrow in **Figure S12**. Step (0) is the transformation from the reference $\text{Pt}_{13}\text{H}_6/\gamma\text{-Al}_2\text{O}_3(100)$ system to the deformed $\text{Pt}_{13}\text{H}_6/\gamma\text{-Al}_2\text{O}_3(100)$ system induced by 4-MCHe after MD, which corresponds to +41 kJ/mol, confirming that the

reference catalyst model is the most stable one in absence of adsorbed 4-MCHe. For step (1), the energy to separate the metal cluster and the support is highly positive (+980 kJ/mol). Comparing to step (1'), it is found that after AIMD the interaction (+849 kJ/mol) between the Pt cluster and the γ -Al₂O₃ (100) surface is weakened. These positive energies are mostly compensated by the final recombination energies at step (6) and (6'). However, with adsorbed 4-MCHe, the interaction energy after AIMD is reinforced (+862 kJ/mol), whereas the one without AIMD is weakened. Steps (2'') and (3'') correspond to the deformation energy of the support and the cluster (both isolated) with and without after AIMD. Whereas the deformation energy of the support is modest, the cluster after MD becomes more stable by -81 kJ/mol. Steps (4) and (4') are the dehydrogenation of MCH_(g) to 4-MCHe, respectively on the cluster without and with MD: both exhibit similar energy variation. As for step (3'''), the deformation of the cluster with adsorbed MCHe in step (5) is exothermic by -94 kJ/mol. Finally, the interaction between the support and the cluster with the adsorbed MCHe is reinforced for the cluster with AIMD: 862 kJ/mol for step (6') compared to 849 kJ/mol for step (1'). Without AIMD, the trend is the reverse: 953 kJ/mol for step (6) compared to 980 kJ/mol for step (1). Once the system is recombined, a compensation effect occurs which levels the stability discrepancy (-4 kJ/mol for step (7)).

9.3 C-H bond cleavages

Table S13. Thermodynamic and kinetic data (kJ/mol, PBE-dDsC level) for the C-H bond cleavage at 625K.

		Forward reaction								Backward reaction				
Elementary step	Transition States	$\Delta_r E$	$\Delta_r H$	$T\Delta_r S$	$\Delta_r G$	$\Delta_r E^\ddagger$	$\Delta_r H^\ddagger$	$T\Delta_r S^\ddagger$	$\Delta_r G^\ddagger$	$\Delta_r E^\ddagger$	$\Delta_r H^\ddagger$	$T\Delta_r S^\ddagger$	$\Delta_r G^\ddagger$	
A \rightarrow B	TS_a	-42	-48	-7	-41	31	19	-14	33	73	67	-7	74	
B \rightarrow C	TS_b	-18	-27	3	-31	88	74	4	70	106	101	1	101	
D \rightarrow E	TS_d	6	-6	-12	6	113	98	3	95	107	104	15	89	
G \rightarrow H	TS_g	-70	-78	-4	-74	47	33	0	33	118	111	4	107	
J \rightarrow K	TS_j	-41	-52	6	-58	45	34	-10	44	86	86	-17	103	
L \rightarrow M	TS_l	-23	-30	16	-46	107	94	7	87	130	124	-8	132	

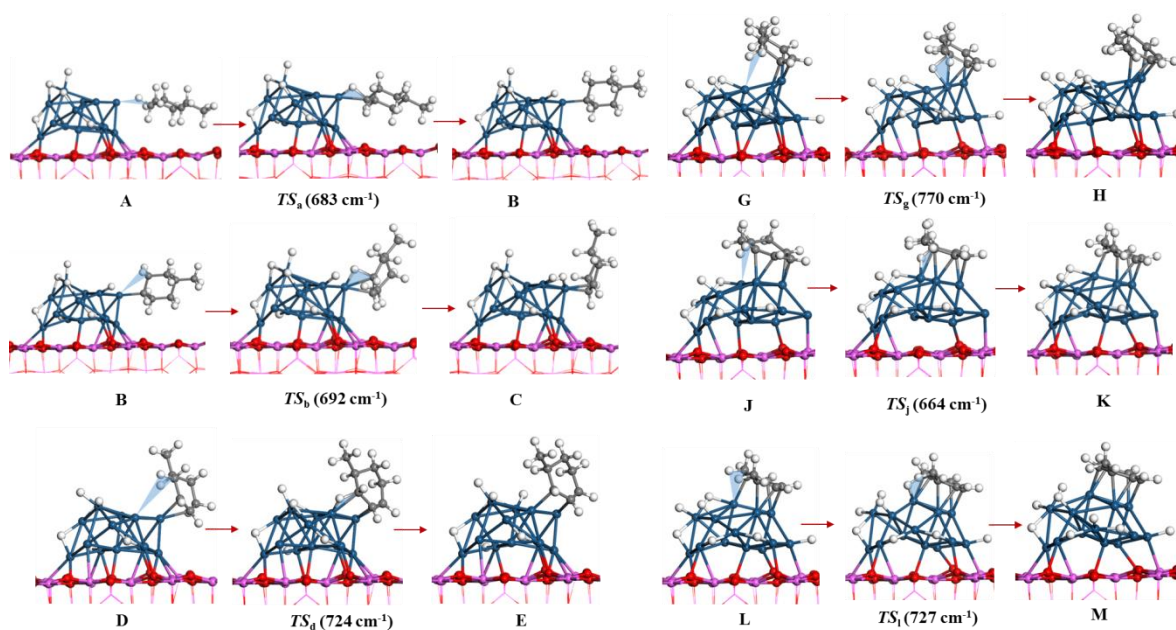


Figure S13. Configurations (PBE-dDsC level) of the six transition states of C-H bond cleavage steps. The unique imaginary vibrational frequency is given in parenthesis. The unique imaginary frequency of each *TS* is given in parenthesis.

Color legend: aluminum (pink balls), oxygen (red balls), platinum (dark blue balls), carbon (dark grey balls), hydrogen (white balls).

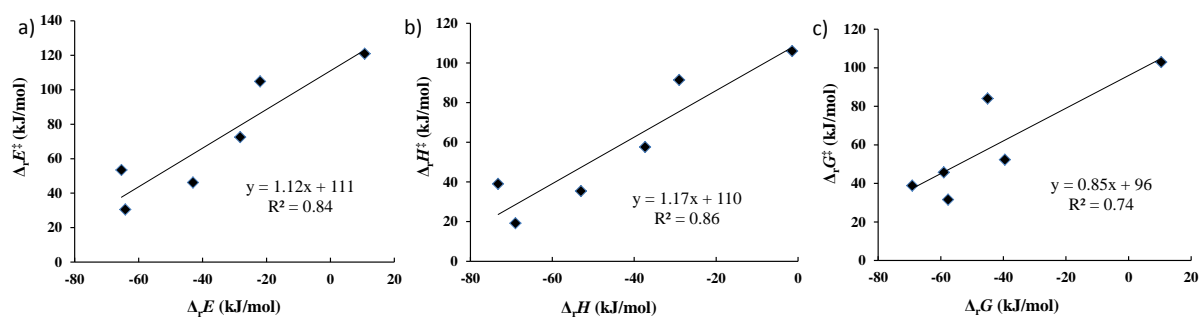


Figure S14. Brønsted–Evans–Polanyi (BEP) linear relationships based on a) electronic energy, b) enthalpy, c) free energy for C-H bond cleavage steps at PBE level

References

- (1) Sabbe, M. K.; Canduela-Rodriguez, G.; Reyniers, M. F.; Marin, G. B.: Dft-Based Modeling of Benzene Hydrogenation on Pt at Industrially Relevant Coverage. *J. Catal.* **2015**, *330*, 406-422.
- (2) Ma, H. Y.; Wang, G. C.: Theoretical Study of 1,3-Cyclohexadiene Dehydrogenation on Pt (111), Pt₃Sn/Pt (111), and Pt₂Sn/Pt (111) Surfaces. *J. Catal.* **2011**, *281*, 63-75.
- (3) Morin, C.; Simon, D.; Sautet, P.: Intermediates in the Hydrogenation of Benzene to Cyclohexene on Pt(111) and Pd(111): A Comparison from Dft Calculations. *Surf. Sci.* **2006**, *600*, 1339-1350.
- (4) Morin, C.; Simon, D.; Sautet, P.: Chemisorption of Benzene on Pt(111), Pd(111), and Rh(111) Metal Surfaces: A Structural and Vibrational Comparison from First Principles. *J. Phys. Chem. B* **2004**, *108*, 5653-5665.
- (5) Hu, C. H.; Chizallet, C.; Mager-Maury, C.; Corral-Valero, M.; Sautet, P.; Toulhoat, H.; Raybaud, P.: Modulation of Catalyst Particle Structure Upon Support Hydroxylation: Ab Initio Insights into Pd₁₃ and Pt₁₃/Γ-Al₂O₃. *J. Catal.* **2010**, *274*, 99-110.